International Journal of
Molecular Sciences

MDPI

Article

RETRACTED: Optimized Conjugation of Fluvastatin to HIV-1 TAT Displays Enhanced Pro-Apoptotic Activity in HepG2 Cells

Lamya H. Al-Wahaibi [1], Muneera S. M. Al-Saleem [1], Osama A. A. Ahmed [2,*], Usama A. Fahmy [2], Nabil A. Alhakamy [2], Basma G. Eid [3], Ashraf B. Abdel-Naim [3], Wael M. Abdel-Mageed [4], Maha M. AlRasheed [5] and Gamal A. Shazly [6]

1 Department of Chemistry, Science College, Princess Nourah Bint Abdulrahman University, Riyadh 11671, Saudi Arabia; lhalwahaibi@pnu.edu.sa (L.H.A.-W.); msalsaleem@pnu.edu.sa (M.S.M.A.-S.)
2 Department of Pharmaceutics, Faculty of Pharmacy, King Abdulaziz University, Jeddah 21589, Saudi Arabia; uahmedkauedu.sa@kau.edu.sa (U.A.F.); nalhakamy@kau.edu.sa (N.A.A.)
3 Department of Pharmacology and Toxicology, Faculty of Pharmacy, King Abdulaziz University, Jeddah 21589, Saudi Arabia; beid@kau.edu.sa (B.G.E.); abnaim@yahoo.com (A.B.A.-N.)
4 Department of Pharmacognosy, College of Pharmacy, King Saud University, P.O. Box 2457, Riyadh 11451, Saudi Arabia; wabdelmageed@ksu.edu.sa
5 Department of Clinical Pharmacy, College of Pharmacy, King Saud University, P.O. Box 2457, Riyadh 11451, Saudi Arabia; mahalrasheed@ksu.edu.sa
6 Department of Pharmaceutics, College of Pharmacy, King Saud University, P.O. Box 2457, Riyadh 11451, Saudi Arabia; gaahmed@ksu.edu.sa
* Correspondence: oaahmed@kau.edu.sa; Tel.: +966-5-9912-0686

Received: 29 May 2020; Accepted: 7 June 2020; Published: 10 June 2020; Retracted: 8 November 2024

Abstract: Accumulating evidence indicates that statins reduce the risk of different cancers and inhibit the proliferation of liver cancer cells. This study aims to explore whether the electrostatic conjugation of optimized fluvastatin (FLV) to human immunodeficiency virus type 1 (HIV-1) trans-activator transcription peptide (TAT) would enhance the anti-proliferative activity against HepG2 cells. FLV–TAT conjugation was optimized to achieve the lowest size with highest zeta potential. Nine formulae were constructed, using a factorial design with three factors—FLV concentration, TAT concentration, and pH of the medium—while the responses were zeta potential and size. The optimized formula showed a particle size of 199.24 nm and 29.14 mV zeta potential. Data indicates that conjugation of FLV to TAT (optimized formula) significantly enhances anti-proliferative activity and uptake by HepG2 cells when compared to raw FLV. Flow cytometry showed significant accumulation of cells in the pre-G phase, which highlights higher apoptotic activity. Annexin V staining indicated a significant increase in total cell death in early and late apoptosis. This was confirmed by significantly elevated caspase 3 in cells exposed to FLV–TAT preparation. In conclusion, the FLV–TAT optimized formula exhibited improved anti-proliferative action against HepG2. This is partially attributed to the enhanced apoptotic effects and cellular uptake of FLV.

Keywords: fluvastatin; HIV-TAT; HepG2 cells; apoptosis; cationic peptide; cancer

1. Introduction

Liver cancer is a slow progressive disease, which is currently the world's sixth most common cancer. The second cause of cancer-related mortality is liver cancer, as reported by the World Health Organization [1,2]. The development of liver cancer has been linked to the hepatitis C virus, high blood sugar levels, fatty liver disease, obesity, and cholesterol dysregulation [3,4]. As the incidence of these

This paper has been retracted.
A retraction notice was published on 8 November 2024 in *International Journal of Molecular Sciences* **2024**, *25*, 12012; doi:10.3390/ijms252212012

predisposing factors is expected to rise over the coming years, there is a need to explore different strategies that may enhance current available treatments.

The high availability, ease of handling, and stable phenotype of hepatoma cells makes them suitable candidates for in vitro studies. In addition, these cells have a long lifespan, which is almost unlimited [5]. HepG2 is a type of hepatoma in humans with various functions, including plasma protein synthesis and secretion, metabolism of triglycerides and cholesterol, metabolism and transport of lipoproteins, and the synthesis of glycogen and bile [6]. Therefore, HepG2 cells are commonly employed in pharmaco-toxicological research [7].

One possible intervention is the use of cholesterol-reducing statins and 3-hydroxy-3-methylglutaryl coenzyme A (HMG-CoA) reductase inhibitors. These agents ameliorate dyslipidemia and lower the risk of various heart diseases [8]. A number of observational studies further support the idea that the risk of liver cancer is reduced by statins [9,10]. Since the liver is the organ of cholesterol synthesis, statins ordinarily target the liver and are mainly sequestered in liver tissue. Several studies have shown that statins reduce angiogenesis and metastasis, and promote apoptosis [11–13]. Clinical studies have shown that the incidence of hepatocellular carcinomas is reduced by statins [14,15]. In particular, fluvastatin (FLV) has shown utility against human hepatocellular carcinoma, prostate carcinoma, and breast cancer cells [16–18]. A study by Zhang et al. found that FLV caused apoptosis in hepatic carcinoma cells [17].

HIV-1 transactivator of transcription peptide (TAT) is a cationic cell penetrating peptide (CPP) that has gained attention over the past few years [19–27]. This regulatory protein can incorporate diverse molecules with therapeutic potential, such as antibodies, liposomes, nanoparticles, nucleic acids, and small peptides [28–32]. The ability of TAT to effectively penetrate cells allows it to efficiently deliver various exogenous substances [33–35]. TAT can also decrease the proliferation of cancer cells, and can therefore serve as a valuable carrier of chemotherapeutic agents [36]. Hence, the goal of the study was to determine whether the electrostatic conjugation of optimized FLV to TAT would enhance the anti-proliferative activity against HepG2 cells.

2. Results

2.1. FLV–TAT Formulation and Characterization

2.1.1. Particle Size (Y1)

The particle size of the prepared nanoparticle formulations was 87 and 1675 nm for runs 5 and 7, respectively as shown in Table 1. The results displayed in Table 2 show the factorial analysis of variance (ANOVA) of FLV concentration (X1) on the particle size (Y1). Equation (1) gives the prediction model that was used to correlate variables with the obtained sizes. Figure 1A shows the standardized Pareto chart for the effect of factors X1, TAT concentration (X2), and pH of the medium (X3), as well as their interaction terms on Y1. A Pareto chart is used to show the factors and their interaction term effects, in descending hierarchy of importance, on particle size. A vertical dashed reference line (dotted line) on the chart signifies the critical *p*-value of 0.05. A statistically significant effect would surpass the vertical line. The Pareto chart shows the significant effect of X1 on Y1. Figure 1C,E shows the influence of factors on particle size using contour and the response surface plots, respectively. Contour and response surface plots were determined graphically, utilizing the Minitab Statistical program to reveal the relationship between the investigated variables and particle size that indicates the direct relationship between X1 and Y1.

$$\text{Particle size (Y1)} = -98.00 + 117.00X1 + 34.50X2 + 10.00X3 + 7.50(X1 \times X2) + 2.24(X1 \times X3) - 1.72(X2 \times X3) - 2.67(X1 \times X2 \times X3) \quad (1)$$

Table 1. Formulation variables fluvastatin concentration (XI), transcription peptide concentration (X2), and pH of the medium (X3) of FLV–TAT formulations and their observed responses (particle size (Y1) and zeta potential (Y2)), as suggested by the factorial design.

Run #	FLV (mM)	TAT (mM)	pH	Particle Size * (nm)	Zeta Potential * (mV)
1	1	1	8	134 ± 9.3	20.10 ± 2.4
2	10	1	2	1200 ± 96.2	18.00 ± 1.1
3	1	10	8	196 ± 23.2	29.40 ± 3.5
4	10	1	8	1224 ± 112.7	18.40 ± 2.1
5	1	1	2	87 ± 10.1	13.05 ± 1.6
6	5.5	5.5	5	544 ± 34.7	21.00 ± 1.7
7	10	10	2	1675 ± 143.2	4.80 ± 0.3
8	10	10	8	167 ± 13.2	25.05 ± 2.1
9	1	10	2	386 ± 22.1	47.00 ± 2.9

* Data represent mean of three independent replicates ± SD.

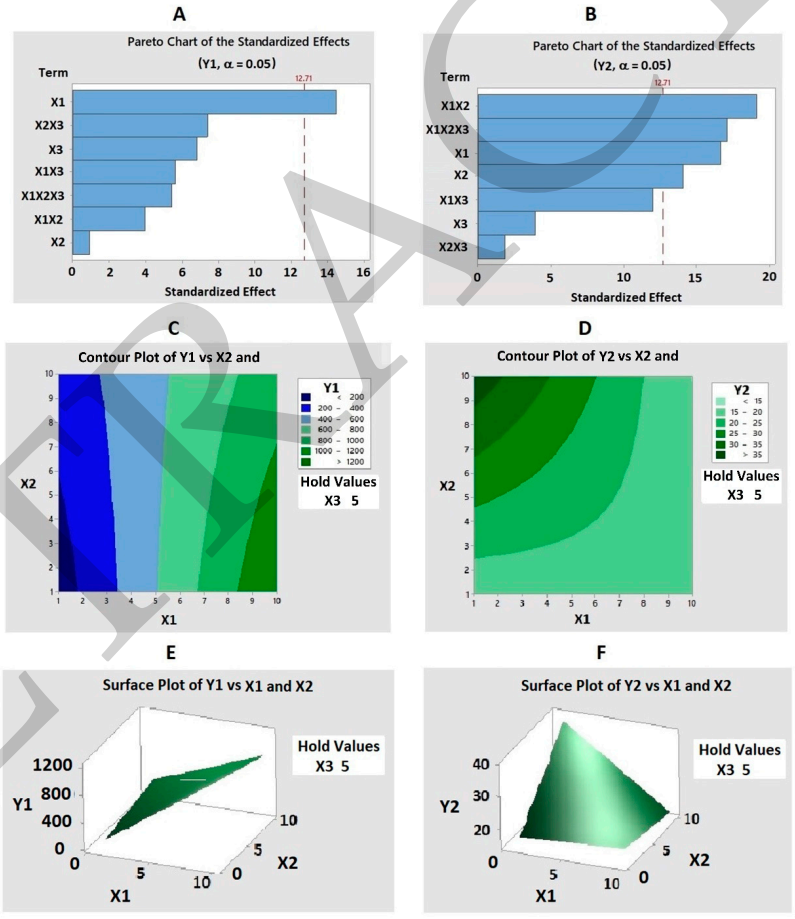

Figure 1. Pareto charts (**A**,**B**) showing the vertical dashed reference line of significance ($p < 0.05$). Contour plots (**C**,**D**) and three-dimensional (3D) response surface plots (**E**,**F**) for Y1 and Y2, showing the effects of X1, X2, and X3, as well as their combined effects on Y1 and Y2. Abbreviations: X1, FLV concentration (mM); X2, TAT concentration (mM); X3, pH of the medium Y1, particle size (nm); Y2, zeta potential (mV); the interaction term between the factors X1X1, X2X2, and X3X3 are the quadratic terms between the factors; X1X2, X1X3, X2X3, and X1X2X3 are the interaction terms of the investigated factors.

Table 2. Statistical analysis of variance (ANOVA) of the responses (Y1 and Y2) results.

Factors	Y1		Y2	
	***F*-Value**	***p*-Value**	***F*-Value**	***p*-Value**
X1	209.95	0.044 *	277.35	0.038 *
X2	0.86	0.525	199.24	0.045 *
X3	46.34	0.093	15.09	0.160
X1X2	15.57	0.158	366.87	0.033 *
X1X3	31.48	0.112	144.00	0.053
X2X3	54.78	0.085	3.41	0.316
X1X2X3	29.36	0.116	292.94	0.037 *
R^2	99.74%		99.92%	
Adj. R^2	97.95%		99.38%	

* significant effect of factors on individual responses. Abbreviations: X1: FLV concentration (mM); X2: TAT concentration (mM); X3: pH of the medium; Y1: particle size (nm); Y2: zeta potential (mV); X1X2, X1X3, X2X3 and X1X2X3 are the interaction term between the factors; R^2: *R*-squared; Adj. R^2: adjusted *R*-squared.

2.1.2. Zeta Potential (Y2)

For all the studied formulations, zeta potential (Y2) values ranged from 4.8 mV for formula 7 to 47 mV for formula 9 (Table 1). It was clear that X1 and X2 had a major role in the observed difference in the zeta potential of the FLV–TAT formulations. X1 and X2 had major inverse effects on Y2 (Table 2), as confirmed by multiple regression analyses. Furthermore, the two-way interaction term of X1 and X2 significantly affected Y2 (p-value = 0.033). The three-way interaction term of X1, X2, and X3 significantly affected Y2 (p value = 0.037) (Table 2). Equation 2 shows the Y2 value prediction equation. The Pareto chart (Figure 1B) shows the significant effect of the investigated factors X1, X2, X3 and their interactions on Y2. The relationship between the Y2 factors are given in the contour (Figure 1D) and response surface plots of Y2 (Figure 1F).

$$\text{Zeta potential (Y2)} = 4.340 + 1.562X1 + 5.450X2 + 1.846X3 - 0.765(X1 \times X2) - 0.215(X1 \times X3) - 0.548(X2 \times X3) + 0.092(X1 \times X2 \times X3) \quad (2)$$

2.2. Optimization of FLV–TAT Formulations

After analysis of the results generated from the nine runs from (Table 1) that were prepared, and their particle size and zeta potential values practically measured. Software was used to aid in optimizing FLV- TAT formulation that was prepared and evaluated. Independent factor combinations for the optimized FLV- TAT formulation had a particle size of 199.24 nm and a zeta potential of 29.14 mV. Table 3 shows the observed (actual) and predicted (deduced by the software) values of the optimized formula. The observed values are the values that were recorded practically (actual results) after preparation of the optimized formula. On the other hand, the predicted values are the values deduced (suggested) by the software after analysis of the results generated from the nine runs. No considerable residuals were apparent from the observed and predicted responses (Y1 and Y2).

Table 3. Optimized calculated variables and observed, predicted, and residual values for responses (Y1 and Y2).

Factor	Optimized	Response	Predicted	Observed	Residual
X1	1.00	**Y1 (nm)**	193.72	199.24	5.52
X2	10.00				
X3	7.78	**Y2 (mv)**	30.01	29.14	0.87

X1: FLV concentration (mM); X2: TAT concentration (mM), X3: pH of the medium; Y1: particle size (nm); Y2: zeta potential (mV).

2.3. Fourier-Transformed Infrared Spectroscopy Investigation of the Optimized FLV–TAT Complex

FLV showed a broadband peak at 3100–3500 cm^{-1} due to alcoholic and carboxylic hydroxyl groups (Figure 2). TAT showed a strong broadband at 3300–3400 cm^{-1} of NH stretching related to NH_2, amide, and guanidine groups, which are associated with a strong peak around 1500–1700 cm^{-1}, as well as broadbands related to NH bending at 1580–1650 cm^{-1}, amidic C=O stretching at 1680 cm^{-1}, and C=N stretching of guanidine at 1690 cm^{-1}. FLV-TAT showed a very broadband extended at 3000–3700 cm^{-1}; also, characteristic bands at 1500–1700 cm^{-1} of TAT were sharply reduced in intensity in FLV-TAT, confirming the interaction of the main function groups of FLV and TAT together like a complex formation (Figure 2).

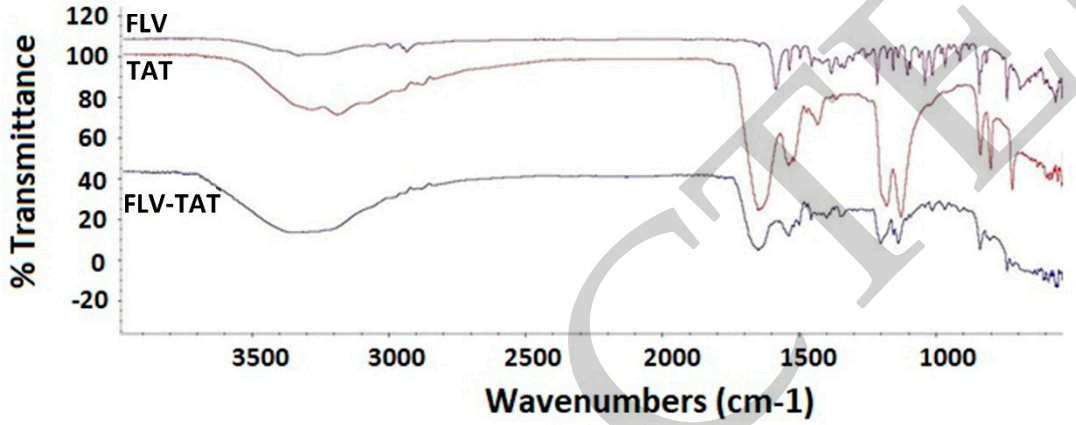

Figure 2. FLV, TAT, and FLV–TAT complex FTIR spectra.

2.4. Anti-Proliferative Activity (In Vitro)

To assess the anti-proliferative action on HepG2 cells, various concentrations of FLV, TAT, and FLV–TAT were used. As presented in Figure 3, IC_{50} values for the treatment groups were determined as follows: FLV = 39.66 ± 2.02 µM and TAT = 14.1.43 ± 1.61 µM. However, the conjugated formula of FLV–TAT (1:10 FLV/TAT, respectively) exhibited significantly enhanced, proliferation-inhibiting activity, with IC_{50} value of 1.76 ± 0.25 µM. The combination index (CI) of FLV combined with TAT was found to be 0.29, indicating a synergistic cytotoxic effect of FLV alone. The cytotoxic activities were compared to the standard reference cytotoxic compound mitomycin, which showed an IC_{50} of 0.9 ± 0.1 µM. All treatments using the same concentrations were tried against the human embryonic kidney 293 (HEK 293) cells, and all IC_{50} values were above 100 µM (FLV = 142.66 ± 11.34 µM, TAT = 131 ± 9.82 µM, and FLV–TAT = 107.52 ± 8.55 µM).

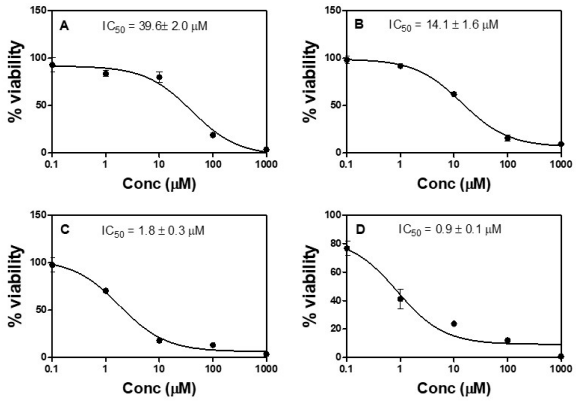

Figure 3. IC_{50} of FLV (**A**), TAT (**B**), optimized FLV–TAT (**C**), and Mitomycin (**D**) in HepG2 cells. All incubation continued for 48 h; data represent the mean of six independent replicates ± SD.

2.5. Cellular Uptake

Figure 4 illustrates quantitative cellular uptake of FLV that had been entrapped in the HepG2 cells after exposure to raw FLV (0.1 μM) or FLV–TAT (0.1 μM–1 μM, respectively) after 2 and 4 h. At 2 h incubation time, cells challenged with FLV–TAT showed significant improvement in FLV uptake (35.2% ± 5.6%) when compared with raw FLV treatment (16.91% ± 1.7%). At 4 h incubation, FLV–TAT showed similar enhancements in cellular uptake (88.4% ± 8.2%), as compared with FLV raw (37.21% ± 3.1%).

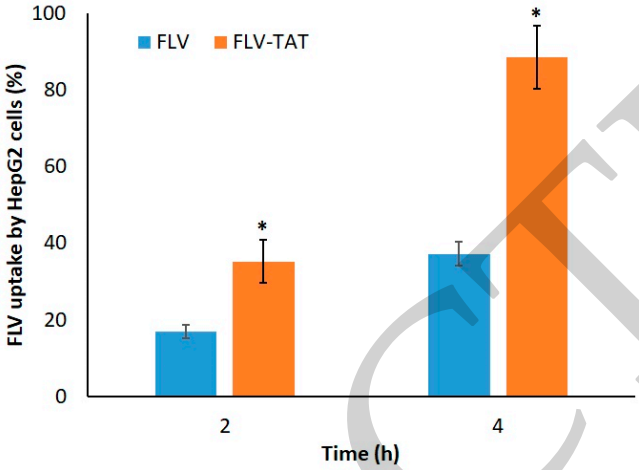

Figure 4. Percentage cellular uptake of FLV after 2 and 4 h for raw FLV and optimized FLV–TAT. Data represent mean of six independent replicates ± SD. * Significantly different ($p < 0.05$) relative to corresponding FLV, as determined by Student's *t*-test.

2.6. In Vitro DNA Flow Cytometry Analysis

As given in Figure 5A, control HepG2 cells exhibited proliferative properties, with 54% ± 3.8 % at the G0/G1 phase, 33% ± 2% at the S phase, 12.6% ± 1.2% at the G2-M phase, and only 1.36% ± 0.02% at pre-G1 phase. Incubation in FLV (0.1 μM), TAT (1 μM), and FLV–TAT (0.1 μM–1 μM, respectively) slowed the proliferation of HepG2 cells and induced their accumulation at the pre-G1 apoptotic phase (Figure 5B–D). This accumulation amounted to 7.26% ± 0.9%, 8.36% ± 0.5% and 16.12% ± 1% for FLV, TAT, and FLV–TAT, respectively. In addition, FLV–TAT-treated cells showed significant accumulation in G2-M phase. Different cell cycle stages are compared in Figure 5E,F.

2.7. Annexin V staining

To confirm the observed apoptosis, an annexin V test was carried out, and the percentage of HepG2 cells that stained positive was calculated for the control, FLV, TAT, and FLV–TAT groups (Figure 6A–D). It is apparent that FLV–TAT had an obvious increase in early, late, and total cell death relative to the other studied groups. Figure 6E shows different types of cell death.

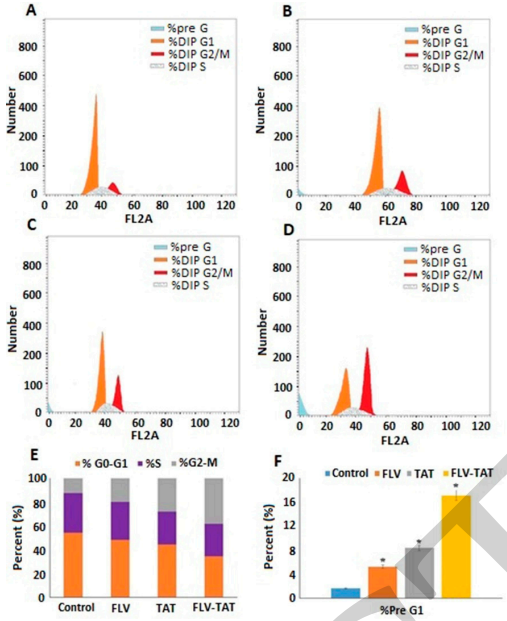

Figure 5. Impact of the treatments on the cell cycle phases. (**A**) Control, (**B**) raw FLV, (**C**) TAT, (**D**) optimized FLV–TAT, and (**E**,**F**) graphical presentation of each phase. All incubation continued for 48 h. Data represent the mean of six independent replicates ± SD. * Significantly different ($p < 0.05$) relative to the corresponding control.

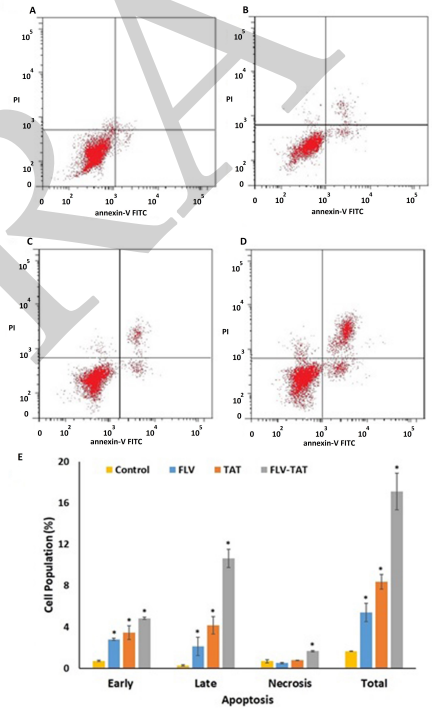

Figure 6. Impact of the treatments on the annexin V- and FITC (fluorescein isothiocyanate)-positive-staining HepG2 cells. (**A**) Control, (**B**) raw FLV, (**C**) TAT, (**D**) optimized FLV–TAT, and (**E**) graphical presentation of early and late apoptotic, necrotic, and total cell death. All incubation continued for 48 h. Data represent mean of six independent replicates ± SD. * Significantly different ($p < 0.05$) relative to the corresponding control.

2.8. Caspase 3 Enzyme Assay

Assessment of caspase 3 concentration in HepG2 cells indicates a significantly higher concentration of the enzyme in FLV–TAT compared with raw FLV, TAT, and control groups. Caspase 3 concentration was found to be 198.6 ± 19.9, 273.9 ± 17.1, 454.2 ± 26.7 pg/mL for FLV, TAT, and FLV–TAT, respectively, as shown in Figure 7.

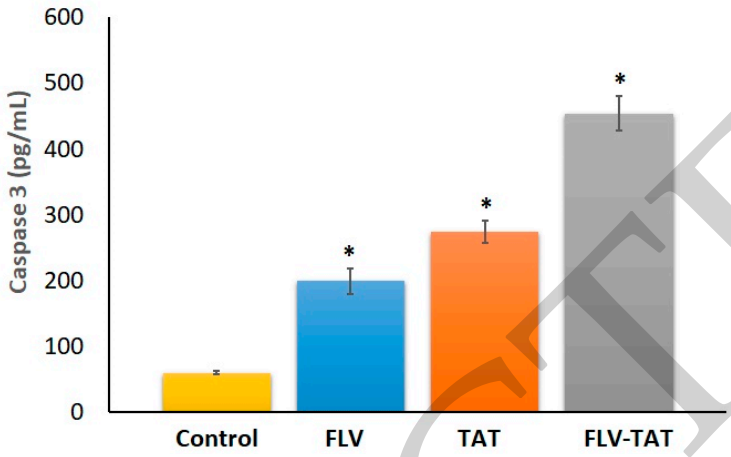

Figure 7. Impact of FLV, TAT, and optimized FLV–TAT on caspase 3 enzyme concentrations in HepG2 cells. All incubation continued for 48 h. Data represent mean of six independent replicates ± SD. * Significantly different ($p < 0.05$) relative to the corresponding control.

3. Discussion

Physicians are often reluctant to prescribe statins in patients with liver diseases, due to various concerns. One of these concerns is the possibility of developing liver injury. Emerging evidence from both clinical and preclinical trials has shown the potential utility of statins in hepatocellular carcinoma prevention [37]. This necessitates the search for new formulations of statins with enhanced activity, and consequently lower doses and incidence of adverse effects. Observational studies on humans with hepatitis C indicates that FLV is associated with dose-dependent decreases in hepatocellular carcinoma [38]. CPPs have been introduced as applicable drug delivery tools, proteins, and plasmid DNA and RNA to the intracellular environment. In particular, it has been demonstrated that HIV-1 TAT-derived CPPs are effective in delivering many types of drug molecules [39]. Exploration of the potential enhancement of HepG2 cell death by FLV loaded in TAT was the main aim of this study. TAT as a CPP showed the ability to translocate the different therapeutic molecules into living cells [40]. In addition, the focus on CPPs as an alternative strategy of delivering the therapeutic load against a variety of diseases to overcome drug delivery limitations has gained more attention [41]. TAT as a positively charged peptide improves cellular translocation of FLV through cell membrane attraction, which stimulates a receptor-independent pathway through receptor-mediated endocytosis [26,30,34,42].

The variables that affect the process of formula preparation must be identified. A tool is required to investigate the effect of these variables on the formula at the same time [43,44]. If investigated manually, i.e., the one factor at a time method rather than multiple factors simultaneously, this could cost time and effort. Experimental design software is beneficial in this regard [45]. Factorial design offers more information at lower effort and cost. Accordingly, optimization of the formulation factors (X1–X3) that affect both Y1 and Y2 are essential for therapeutic agent delivery into living cells.

The optimized FLV–TAT formula deduced by the experimental design showed, after preparation, a particle size of 199.24 nm and a zeta potential of 29.14 mV, i.e., near the optimal zeta potential (+/− 30 mV) for particle stability. Positively charged nanobodies (+29.14 mV zeta potential) enhanced cellular translocation and improved the stability of the prepared optimized formulation when compared with raw FLV [46]. Zeta potential is one of the important indicators for colloidal dispersion stability.

The value of zeta potential affects formulation specification, quality, and performance. In other words, zeta potential maintains a more consistent product.

FLV carboxylic groups are conjugated to the surface of the amino groups of TAT in sequence through carbodiimide coupling. Thus, one equivalent of TAT with 10 amino groups will be coupled with 10 carboxylic groups of 10 equivalent FLVs. This new carbodiimide coupling refers to the consumption of NH_2 by TAT and COOH by FLV, and this was confirmed by the strong broadening and decrease in intensity of the H-bonding band at 3300–3700 cm^{-1}.

Generally, hepatic cell lines offer many advantages, as they grow continuously, have an almost unlimited lifespan, and have quite a stable phenotype. The availability and simple culture conditions of liver cancer cell lines offer another advantage over primary hepatocytes. These features make hepatic cell lines potentially appropriate for screening purposes [47]. In particular, HepG2 cells have characteristic genotypic and phenotypic features, such as being highly differentiated, that increase their suitability for screening the cytotoxicity of new potential chemical compounds at the lead generation phase [48]. In the current study, proliferation of HepG2 hepatocellular carcinoma cells was inhibited by FLV, as indicated by the 3-(4,5-dimethylthiazol-2-yl)-2,5-diphenyltetrazolium bromide (MTT) assay results. The assay measures the presence of live cells containing active, nicotinamide adenine dinucleotide phosphate (NADPH)-dependent oxidoreductase enzymes that catalyze the cleavage of tetrazolium salt MTT semi-quantitatively. Hence, it could be a measurement of surviving cells. FLV–TAT showed the most potent anti-proliferative activity. Several reports have supported this observed anti-proliferative activity of FLV against different cancer cells—for example, against pancreas [49], breast [50], glial [51], and colorectal [52] cancer cells. FLV has been shown to decrease resistance of melanoma [53], breast, and ovarian cells [54]. Further, FLV has shown strong growth-inhibitory and anti-metastatic effects on hepatocellular carcinoma cells [18,55]. FLV and other statins inhibit 3-Hydroxy-3-Methylglutaryl-CoA reductase. An upregulation of the mevalonic acid (MVA) pathway occurs due to cellular deprivation of mevalonic acid end products [56]. Cellular proteins, such as p21rhoA and p21ras, are not geranylated and farnesylated due to FLV anti-proliferative activities. The phosphorylation of p42ERK2/mitogen-activated protein kinase and activity of p38 MAPK are also indirectly blocked [57,58]. In addition, FLV cytotoxicity can be attributed to the reported statins' ability to alter the non-cellular components of tumor cells' microenvironments as inflammatory cytokines [59]. FLV has been reported to have anti-inflammatory activities, and inhibits release of induced cytokines in different in vitro models [60,61]. Interestingly, the plain TAT showed significant proliferation-inhibiting activity. A previous report, which examines the cytotoxicity of cell-penetrating peptides, including TAT against Chinese hamster ovary (CHO) cells, further supports this notion [62]. TAT can effectively recruit proteins that induce apoptosis, therefore causing cell death [63,64]. It causes the upregulation of tumor necrosis factor (TNF)-related, apoptosis-induced ligands (TRAILs), as well as caspase 3 [65]. It also causes the upregulation of Fas, Fas ligand (FasL/CD95L), and TNF-a [66]. Both Fas/FasL system and caspase 3 initiate and execute apoptotic cell death [67]. Thus, the observed, enhanced, proliferation-inhibiting activity of the prepared formula may be substantiated by the cytotoxic capabilities of TAT. To further investigate the enhanced anti-proliferative properties of FLV–TAT, cellular uptake of FLV was assessed using 0.1 μM. The IC_{50} of FLV–TAT in HepG2 cells has been found to be 1.8 μM. Thus, the chosen concentration is highly non-toxic to HepG2 cells. Further, this concentration was based on a preliminary experiment, and proved to be optimal under our experimental conditions; it complied with the sensitivity of the analytical methods used. Although our data indicate that about 80% of FLV–TAT was taken into cells at 4 h, only 50% apoptotic cells were observed at 24 h. This may be due to the lower concentrations used in the cellular uptake experiment (0.1 μM raw FLV and an equivalent concentration of FLV–TAT) compared to the IC_{50} values (14.1 and 1.8 μM, respectively) used in the apoptosis experiment. Also, HepG2 cells have a doubling time of 48 h [68]. Therefore, an estimated small, undefined surviving fraction after challenge with FLV–TAT is expected to proliferate and reach 50% of the whole cellular population at 24 h. The obtained data indicated that TAT significantly enhanced the cellular uptake of FLV. These results lend additional

support for augmented cytotoxicity against HepG2 cells. Actually, CPPs have been used to enhance the uptake of several anticancer drugs across biological membranes. These included doxorubicin [69,70] and methotrexate [71]. The ability of TAT and CPPs to enhance cellular transport of the bound cargo can be attributed to their highly cationic nature, which facilitates their passage across the negatively charged cell membranes. Mechanisms of internalization have been previously reviewed [72].

The observed enhancement of the anti-proliferative properties of the prepared FLV–TAT formula was further substantiated by assessing its impact on cell cycle phases. DNA flow cytometric analysis showed that a significant accumulation of HepG2 cells in the G2-M and pre-G1 phases was caused by FLV. These data are supported by a study of Zhang et al. [17], who reported that exposure of hepatocellular carcinoma cells to FLV causes apoptosis and G2-M cell cycle arrest. Also, our results are in line with a previous report indicating accumulated PC3 cells in the pre-G1 phase. Collectively, the obtained results indicate that mechanisms of cell death by FLV and FLV–TAT involve the induction of apoptosis. Furthermore, the binding of FLV to TAT resulted in significantly augmented induction of the pro-apoptotic effects. This deduction is supported by a previous indication that mechanisms of FLV and other statin-induced, hepatocellular carcinoma cell deaths are mediated by apoptosis [73]. Also, FLV has been shown to synergize valproic acid-induced apoptosis in glioblastoma multiforme cell lines [74]. Several explanations have been proposed to explain apoptosis induced by statins in different cancer cells. These have involved the regulation of Akt, Erk, and p38 [75], as well as the induction of p21 [76]. In addition, the apoptosis-inducing nature of TAT cannot be excluded [77]. Annexin V staining confirmed the enhanced apoptotic activity of FLV–TAT relative to raw FLV. This was evident at early and late apoptotic death, in addition to total cell death. This is in line with a previous report highlighting the pro-apoptotic activities of FLV in epithelial ovarian cancer cells, as revealed by Annexin V staining [78]. Essentially, caspase 3 is indispensable for cell apoptosis, regardless of mitochondrial cytochrome c release and caspase 9's role [79]. Therefore, caspase 3 was assessed in HepG2 cells exposed to FLV, TAT, or FLV–TAT in this study. Caspase 3 belongs to the caspase (from cysteine–aspartate protease) family, one of the six families of proteases [80]. It is a key enzyme in the execution of apoptosis. It mediates both intrinsic and extrinsic pathways [81]. The obtained results indicate significantly higher concentrations of caspase 3 in cells incubated with FLV–TAT. The detected FLV–TAT enhancement of caspase 3 is in line with several earlier reports [16,77]. These data provide additional support for augmented pro-apoptotic activities. Moreover, the observed augmentation in the cytotoxicity of FLV by conjugation to TAT highlights a potential role for TAT. Thus, the role of TAT alone cannot be excluded.

4. Materials and Methods

4.1. Materials

The Egyptian International Pharmaceutical Industries Company EIPICO (EIPICO, 10th of Ramadan City, Cairo, Egypt) kindly gifted the FLV. TAT protein was obtained from Chengdu Youngshe Chemical Co., Ltd. (Chengdu Youngshe Chemical Co., Chengdu, China). HepG2 Cell Line human and HEK 293 Cell Line human were purchased from Sigma-Aldrich (Sigma-Aldrich Co., St. Louis, MO, USA). Chemicals were of analytical grade.

4.2. FLV- TAT Formulations: Experimental Design

Factorial design was followed for the optimizing FLV formulation. Based on earlier experiments, the factors were micromolar (mM) concentration of FLV (X1), mM concentration of TAT (X2), and pH value (X3), as presented in Table 4. The factors were chosen in order to identify their effect on the particle size (Y1) and zeta potential (Y2) of the formulations. Minitab Statistical Software v.16 (Minitab, LLC, State College, PA, USA) was used. Minimizing Y1 and maximizing Y2 were the goals for the investigation of the dependent variables. Table 4 shows the constraints for the independent variables' levels, as well as the dependent variables.

Table 4. Independent (X1–X3) and dependent (Y1 and Y2) variables of FLV–TAT formulations utilized in the factorial design.

Independent Variables	Unit	Levels		
		−1	0	1
X1	mM	1.0	5.5	10.0
X2	mM	1.0	5.5	10.0
X3	-	2.0	5.0	8.0
Dependent variables	**Unit**	**Constraints**		
		Low	**High**	**Goal**
Y1	nm	87.0	1675.0	Minimize
Y2	mV	4.8	47.0	Maximize

X1: FLV concentration (mM); X2: TAT concentration (mM); X3: pH of the medium; Y1: particle size (nm); Y2: zeta potential (mV).

4.3. Preparation of FLV–TAT Formulations

Formulations of FLV–TAT were prepared according to the above-mentioned design. Different concentrations of FLV and TAT were placed in 20 mL of 0.01 M phosphate buffer with different pH levels, then vortexed for 2 min for dissolution. An aliquot of 1 mL of the prepared complexes was further diluted in 10 mL of the same buffer for the determination of zeta potential and particle size.

4.4. Particle Size and Zeta Potential Determination

Prepared nanoparticles of FLV–TAT formulations were dispersed in water and then measured by a particle size analyzer (Zetatrac; Microtrac Inc., Montgomeryville, PA, USA), which was utilized to analyze zeta potential and particle size. The average particle size and zeta potential were determined from three replicate readings.

4.5. Optimization of FLV–TAT Preparations

Two-way ANOVA and multiple-response optimization (Minitab software) were applied in the statistical analysis of results. A comparison of the zeta potential and particle size of the predicted optimum formulation and the practically prepared formulation was carried out to validate the results.

4.6. Fourier-Transform Infrared Spectroscopy Investigation of the Optimized FLV–TAT Complex

Fourier-transformed infrared (FTIR) analysis was utilized to investigate the interaction between FLV and TAT spectra, which were measured between 4000–400 cm^{-1} using an FTIR spectrophotometer (Nicolet IZ 10, Thermo Fisher Scientific, Waltham, MA, USA).

4.7. Cell Culture

A total of 10 mL RPMI-1640 culture medium (Gibco, Waltham, MA, USA), to which 10% fetal bovine serum (FBS) and glutamine had been added, was used to raise the stock culture. The medium was replaced every 2 days. In addition, 0.25% trypsin–EDTA (ethylenediaminetetraacetic acid) solution (Gibco, Waltham, MA, USA) was used to detach the cells. The cells were then seeded into a sterile 96-well microtiter plates. The cell density of each well was 30,000–50,000. Incubation of the cells was carried out with 5% CO_2 at 37 °C.

4.8. Anti-Proliferative Activity

Cell metabolic activity may be measured using a colorimetric MTT assay. The assay measures the capabilities of nicotinamide adenine dinucleotide phosphate (NADPH)-dependent cellular oxidoreductase enzymes in a reduction of MTT (tetrazolium dye) to formazan, which is violet

and non-soluble [82]. An MTT assay kit (Sigma-Aldrich, St. Louis, MO, USA) was used to study the in vitro anti-proliferative activity of FLV, TAT, and FLV–TAT in HepG2 cells. For evaluating the conjugating of FLV to TAT, a combination index (CI) was determined using Combusyn (ComboSyn, Inc., Paramus, NJ, USA). A CI of less than 1 indicates that the combination has a synergistic effect, whereas CI = 1 or CI > 1 indicates an additive or antagonistic effect, respectively. Additionally, the IC_{50} values of FLV, TAT, and FLV–TAT were determined in non-target cells of non-tumorigenic sources. The same procedures mentioned above were followed using HEK 293 cells cultivated in Eagle's Minimum Essential Medium.

4.9. Cellular Uptake

Cells (HepG2: 1×10^5 cells/dish) were cultured overnight, then were treated with 0.1 µM raw FLV and an equivalent concentration of FLV–TAT in RPMI-1640 culture medium free of FBS. An incubation time of 2 h or 4 h was applied at 37 °C and 5% CO_2. PBS (phosphate buffered saline) was used in washing monolayers (three times), followed by the application of a lysis solution (PBS containing 0.025 % trypsin and 1% tween 20) at 37 °C for half an hour. High-performance liquid chromatography–tandem mass spectrometry (LC-MS/MS) (HPLC Agilent 1200 LC/MS, Agilent Technologies, Santa Clara, CA, USA) was used with electrospray ionization (ESI) to analyze the cell lysates and determine FLV concentration. A Hypersil C18 (150 mm × 4.6 mm, 3µm; Thermo Fisher, Waltham, MA, USA) column was used to separate analytes and the internal standard (pravastatin), with a run time of 10 min in isocratic elution mode. Acetonitrile and water containing 0.01% formic acid and 10 mM ammonium formate at pH 4.1 made up the mobile phase. We applied a multiple reaction monitoring (MRM) technology using the precursor ion 411.9 *m/z* and 224 as a fragment ion [83].

4.10. Analysis of Cell Cycle Progression

A flow cytometer (FACSCalibur, BD Bioscience, Franklin Lakes, NJ, USA) was utilized in the determination of the cell cycle DNA distribution, as previously described [13]. Briefly, approximately 3×10^5 cells/well were seeded in six-well cell culture plates. A concentration of 0.1 µM FLV–TAT was applied to the cells with equivalent concentrations of FLV and TAT for one day. CycleTEST PLUS DNA Reagent Kits (Becton Dickinson Immunocytometry Systems, San Jose, CA, USA) were employed for the analysis of the cell cycle. The DI (DNA index) of each tested preparation was determined in reference to cells with a predetermined content of DNA (PBMCs). Staining was carried out using propidium iodide. Finally, CELLQUEST software (Becton Dickinson Immunocytometry Systems, San Jose, CA, USA) was used, along with a DNA cytometer, to study the distribution of the cell cycle.

4.11. Annexin V Assay

Phosphatidylserine (PS) translocation or externalization occurs prior to the loss of membrane integrity, which occurs with the upcoming stages of cell death due to necrosis or apoptosis. Hence, annexin V staining is used together with propidium iodide (PI) dye to identify cells in late and early apoptosis. PI is unable to penetrate viable cells with intact membranes; however, it can penetrate the membranes of damaged as well as dead cells. Therefore, cells giving negative annexin V and PI stains are taken as viable. On the other hand, cells positive for annexin V and negative for PI are in early apoptosis, whereas cells which are annexin V- and PI-positive are dead or in late apoptosis [84]. The assay was carried out using a detection kit for annexin V–FITC apoptosis (BioVisionResearch Products, Mountain View, CA, USA).

4.12. Assay of Caspase 3 Enzyme

Complete growth medium (RPMI-1640 medium with 10% FBS) was used in culturing HepG2 for 24 h in 96-well plate with 1.8 × 10,000 cells/well. Then, cells were exposed to 0.1 µM FLV–TAT, with equivalent concentrations of FLV or TAT. Cells were lysed by a cell extraction buffer, and a 100 µL sample from each incubation was used for assaying caspase 3, using a commercial kit (USCN Life

Science Inc., Wuhan, Hubei, China). To determine the cleaved caspase 3 content, a CASP3 ELISA Kit #ABIN6574178 (USCN Life Science Inc., Wuhan, China) was used. As per the manufacturer, all components were validated by Western blotting, giving a sensitivity of 0.056 ng/mL with no cross-reactivity or interference between caspase 3 and analogues. The caspase–substrate reaction resulted in an intense color that was assessed by spectrophotometry at a wavelength of 450 nm. The concentration of caspase 3 was determined by comparing the obtained optical density values of samples to a constructed standard curve.

4.13. Statistical Analysis

Data were generated out of at least three independent replicates and are presented as mean ± SD. IBM SPSS statistics program, version 25 (SPSS Inc., Chicago, IL, USA) was used for statistical analysis. Means were compared using unpaired Student's *t*-tests (for cellular uptake investigation) and one-way analysis of variance (ANOVA), followed by Tukey as a post-hoc test, unless otherwise indicated. A result of $p < 0.05$ was considered significant.

5. Conclusions

The FLV–TAT formula was optimized with regard to particle size and zeta potential by experimental statistical methods. The optimized FLV–TAT preparation exhibited improved anti-proliferative activity on HepG2 cells. This can be partially explained by induced apoptosis and enhanced FLV–TAT cellular uptake.

Author Contributions: Conceptualization, O.A.A.A. and U.A.F.; methodology, N.A.A., B.G.E. and G.A.S.; software, W.M.A.-M., A.B.A.-N. and M.M.A.; validation, L.H.A.-W., O.A.A.A., M.S.M.A.-S. and M.M.A.; formal analysis, U.A.F. and B.G.E.; investigation, B.G.E., U.A.F. and A.B.A.-N.; resources, L.H.A.-W. and O.A.A.A.; data curation, U.A.F., B.G.E. and G.A.S.; writing—original draft preparation, O.A.A.A., U.A.F., B.G.E. and L.H.A.-W.; writing—review and editing, L.H.A.-W., M.S.M.A.-S., W.M.A.-M., G.A.S., N.A.A. and M.M.A.; visualization, U.A.F., B.G.E. and O.A.A.A.; supervision, O.A.A.A., A.B.A.-N. and L.H.A.-W.; project administration, L.H.A.-W. and M.S.M.A.-S.; funding acquisition, L.H.A.-W. All authors have read and agreed to the published version of the manuscript.

Funding: This work was funded by the Deanship of Scientific Research at Princess Nourah Bint Abdulrahman University through the Research Groups Program Grant (no. RGP-1440-0014).

Acknowledgments: Authors acknowledge the Deanship of Scientific Research at Princess Nourah bint Abdulrahman University for funding this work through the Research Groups Program Grant (no. RGP-1440-0014).

Conflicts of Interest: The authors declare no conflict of interest.

Abbreviations

FLV	fluvastatin
HIV-1 TAT	human immunodeficiency virus type 1-trans-activator transcription peptide
HMG-CoA	3-hydroxy-3-methylglutaryl coenzyme A
CPP	cationic cell penetrating peptide
ANOVA	analysis of variance
LC-MS/MS	High performance liquid chromatography–tandem mass spectrometry
PS	Phosphatidylserine
NADPH	nicotinamide adenine dinucleotide phosphate

References

1. Sia, D.; Villanueva, A.; Friedman, S.L.; Llovet, J.M. Liver Cancer Cell of Origin, Molecular Class, and Effects on Patient Prognosis. *Gastroenterology* **2017**, *152*, 745–761. [CrossRef]
2. World Health Organization Cancer. Available online: https://www.who.int/health-topics/cancer#tab=overview (accessed on 6 September 2019).

3. Wong, M.C.S.; Jiang, J.Y.; Goggins, W.B.; Liang, M.; Fang, Y.; Fung, F.D.H.; Leung, C.; Wang, H.H.X.; Wong, G.L.H.; Wong, V.W.S.; et al. International incidence and mortality trends of liver cancer: A global profile. *Sci. Rep.* **2017**, *7*, 45846. [CrossRef] [PubMed]
4. Bakiri, L.; Hamacher, R.; Graña, O.; Guío-Carrión, A.; Campos-Olivas, R.; Martinez, L.; Dienes, H.P.; Thomsen, M.K.; Hasenfuss, S.C.; Wagner, E.F. Liver carcinogenesis by FOS-dependent inflammation and cholesterol dysregulation. *J. Exp. Med.* **2017**, *214*, 1387–1409. [CrossRef] [PubMed]
5. Donato, M.; Jover, R.; Gómez-Lechón, M. Hepatic Cell Lines for Drug Hepatotoxicity Testing: Limitations and Strategies to Upgrade their Metabolic Competence by Gene Engineering. *Curr. Drug Metab.* **2013**, *14*, 946–968. [CrossRef] [PubMed]
6. Javitt, N.B. Hep G2 cells as a resource for metabolic studies: Lipoprotein, cholesterol, and bile acids. *FASEB J.* **1990**, *4*, 161–168. [CrossRef]
7. Donato, M.T.; Tolosa, L.; Gómez-Lechón, M.J. Culture and functional characterization of human hepatoma HepG2 cells. In *Protocols in In Vitro Hepatocyte Research*; Springer: New York, NY, USA, 2015; Volume 1250, ISBN 9781493920747.
8. Virani, S.S. Statins in the Primary and Secondary Prevention of Cardiovascular Disease in Women: Facts and Myths. *Texas Hear. Inst. J.* **2013**, *40*, 288.
9. Mansourian, P.G.; Yoneda, M.; Krishna Rao, M.; Martinez, F.J.; Thomas, E.; Schiff, E.R. Effects of statins on the risk of hepatocellular carcinoma. *Gastroenterol. Hepatol. (N. Y.)* **2014**, *10*, 417–426.
10. McGlynn, K.A.; Hagberg, K.; Chen, J.; Graubard, B.I.; London, W.T.; Jick, S.; Sahasrabuddhe, V. V Statin use and risk for primary liver cancer in the clinical practice research datalink. *J. Natl. Cancer Inst.* **2015**, *107*. [CrossRef]
11. Demierre, M.F.; Higgins, P.D.R.; Gruber, S.B.; Hawk, E.; Lippman, S.M. Statins and cancer prevention. *Nat. Rev. Cancer* **2005**, *5*, 930–942. [CrossRef]
12. Browning, D.R.L.; Martin, R.M. Statins and risk of cancer: A systematic review and metaanalysis. *Int. J. Cancer* **2007**, *120*, 833–843. [CrossRef]
13. Alhakamy, N.; Ahmed, O.; Aldawsari, H.; Alfaifi, M.; Eid, B.; Abdel-Naim, A.; Fahmy, U. Encapsulation of Lovastatin in Zein Nanoparticles Exhibits Enhanced Apoptotic Activity in HepG2 Cells. *Int. J. Mol. Sci.* **2019**, *20*, 5788. [CrossRef] [PubMed]
14. German, M.N.; Lutz, M.K.; Pickhardt, P.J.; Bruce, R.J.; Said, A. Statin use is protective against hepatocellular carcinoma in patients with nonalcoholic fatty liver disease: A case-control study. *J. Clin. Gastroenterol.* **2019**. Epub ahead. [CrossRef]
15. Goh, M.J.; Sinn, D.H.; Kim, S.; Woo, S.Y.; Cho, H.; Kang, W.; Gwak, G.; Paik, Y.; Choi, M.S.; Lee, J.H.; et al. Statin Use and the Risk of Hepatocellular Carcinoma in Patients with Chronic Hepatitis B. *Hepatology* **2019**. E print. [CrossRef]
16. Fahmy, U.A. Augmentation of Fluvastatin Cytotoxicity Against Prostate Carcinoma PC3 Cell Line Utilizing Alpha Lipoic–Ellagic Acid Nanostructured Lipid Carrier Formula. *AAPS PharmSciTech* **2018**, *19*, 3454–3461. [CrossRef] [PubMed]
17. Zhang, W.; Wu, J.; Zhou, L.; Xie, H.-Y.; Zheng, S.-S. Fluvastatin, a lipophilic statin, induces apoptosis in human hepatocellular carcinoma cells through mitochondria-operated pathway. *Indian J. Exp. Biol.* **2010**, *48*, 1167–1174.
18. Salis, O.; Okuyucu, A.; Bedir, A.; Gör, U.; Kulcu, C.; Yenen, E.; Kılıç, N. Antimetastatic effect of fluvastatin on breast and hepatocellular carcinoma cells in relation to SGK1 and NDRG1 genes. *Tumor Biol.* **2016**, *37*, 3017–3024. [CrossRef] [PubMed]
19. Via, M.A.; Del Pópolo, M.G.; Wilke, N. Negative Dipole Potentials and Carboxylic Polar Head Groups Foster the Insertion of Cell-Penetrating Peptides into Lipid Monolayers. *Langmuir* **2018**, *34*, 3102–3111. [CrossRef]
20. Traboulsi, H.; Larkin, H.; Bonin, M.A.; Volkov, L.; Lavoie, C.L.; Marsault, É. Macrocyclic Cell Penetrating Peptides: A Study of Structure-Penetration Properties. *Bioconjug. Chem.* **2015**, *26*, 405–411. [CrossRef]
21. Walrant, A.; Cardon, S.; Burlina, F.; Sagan, S. Membrane Crossing and Membranotropic Activity of Cell-Penetrating Peptides: Dangerous Liaisons? *Acc. Chem. Res.* **2017**, *50*, 2968–2975. [CrossRef]
22. Jobin, M.L.; Alves, I.D. On the importance of electrostatic interactions between cell penetrating peptides and membranes: A pathway toward tumor cell selectivity? *Biochimie* **2014**, *107*, 154–159. [CrossRef]
23. Reissmann, S. Cell penetration: Scope and limitations by the application of cell-penetrating peptides. *J. Pept. Sci.* **2014**, *20*, 760–784. [CrossRef] [PubMed]

24. Richard, J.P.; Melikov, K.; Vives, E.; Ramos, C.; Verbeure, B.; Gait, M.J.; Chernomordik, L.V.; Lebleu, B. Cell-penetrating peptides: A reevaluation of the mechanism of cellular uptake. *J. Biol. Chem.* **2003**, *278*, 585–590. [CrossRef] [PubMed]
25. Dupont, E.; Prochiantz, A.; Joliot, A. Penetratin Story: An Overview. *Methods Mol. Biol.* **2011**, *683*, 21–29. [CrossRef]
26. Vendeville, A.; Rayne, F.; Bonhoure, A.; Bettache, N.; Montcourrier, P.; Beaumelle, B. HIV-1 Tat Enters T Cells Using Coated Pits before Translocating from Acidified Endosomes and Eliciting Biological Responses. *Mol. Biol. Cell* **2004**, *15*, 2347–2360. [CrossRef] [PubMed]
27. Lönn, P.; Kacsinta, A.D.; Cui, X.S.; Hamil, A.S.; Kaulich, M.; Gogoi, K.; Dowdy, S.F. Enhancing Endosomal Escape for Intracellular Delivery of Macromolecular Biologic Therapeutics. *Sci. Rep.* **2016**, *6*, 32301. [CrossRef] [PubMed]
28. Bolhassani, A.; Jafarzade, B.S.; Mardani, G. In vitro and in vivo delivery of therapeutic proteins using cell penetrating peptides. *Peptides* **2017**, *87*, 50–63. [CrossRef]
29. Desai, P.; Patlolla, R.R.; Singh, M. Interaction of nanoparticles and cell-penetrating peptides with skin for transdermal drug delivery. *Mol. Membr. Biol.* **2010**, *27*, 247–259. [CrossRef] [PubMed]
30. Park, D.; Lee, J.Y.; Cho, H.K.; Hong, W.J.; Kim, J.J.W.J.; Seo, H.; Choi, I.; Lee, Y.; Kim, J.J.W.J.; Min, S.-J.J.; et al. Cell-Penetrating Peptide-Patchy Deformable Polymeric Nanovehicles with Enhanced Cellular Uptake and Transdermal Delivery. *Biomacromolecules* **2018**, *19*, 2682–2690. [CrossRef]
31. Apte, A.; Koren, E.; Koshkaryev, A.; Torchilin, V.P. Doxorubicin in TAT peptide-modified multifunctional immunoliposomes demonstrates increased activity against both drug-sensitive and drug-resistant ovarian cancer models. *Cancer Biol. Ther.* **2014**, *15*, 69–80. [CrossRef]
32. Farkhani, S.M.; Valizadeh, A.; Karami, H.; Mohammadi, S.; Sohrabi, N.; Badrzadeh, F. Cell penetrating peptides: Efficient vectors for delivery of nanoparticles, nanocarriers, therapeutic and diagnostic molecules. *Peptides* **2014**, *57*, 78–94. [CrossRef] [PubMed]
33. Kristensen, M.; Birch, D.; Nielsen, H.M. Applications and challenges for use of cell-penetrating peptides as delivery vectors for peptide and protein cargos. *Int. J. Mol. Sci.* **2016**, *17*, 185. [CrossRef] [PubMed]
34. Futaki, S.; Nakase, I. Cell-Surface Interactions on Arginine-Rich Cell-Penetrating Peptides Allow for Multiplex Modes of Internalization. *Acc. Chem. Res.* **2017**, *50*, 2449–2456. [CrossRef] [PubMed]
35. Pescina, S.; Ostacolo, C.; Gomez-Monterrey, I.M.; Sala, M.; Bertamino, A.; Sonvico, F.; Padula, C.; Santi, P.; Bianchera, A.; Nicoli, S. Cell penetrating peptides in ocular drug delivery: State of the art. *J. Control. Release* **2018**, *284*, 84–102. [CrossRef]
36. Zhang, S.M.; Sun, Y.; Fan, R.; Xu, Q.Z.; Liu, X.D.; Zhang, X.; Wang, Y.; Zhou, P.K. HIV-1 Tat regulates cyclin B1 by promoting both expression and degradation. *FASEB J.* **2010**, *24*, 495–503. [CrossRef]
37. Vargas, J.I.; Arrese, M.; Shah, V.H.; Arab, J.P. Use of Statins in Patients with Chronic Liver Disease and Cirrhosis: Current Views and Prospects. *Curr. Gastroenterol. Rep.* **2017**, *19*, 43. [CrossRef]
38. Simon, T.G.; Bonilla, H.; Yan, P.; Chung, R.T.; Butt, A.A. Atorvastatin and fluvastatin are associated with dose-dependent reductions in cirrhosis and hepatocellular carcinoma, among patients with hepatitis C virus: Results from ERCHIVES. *Hepatology* **2016**, *64*, 47–57. [CrossRef]
39. Zou, L.; Peng, Q.; Wang, P.; Zhou, B. Progress in Research and Application of HIV-1 TAT-Derived Cell-Penetrating Peptide. *J. Membr. Biol.* **2017**, *250*, 115–122. [CrossRef]
40. Berry, C.C. Intracellular delivery of nanoparticles via the HIV-1 tat peptide. *Nanomedicine* **2008**, *3*, 357–365. [CrossRef]
41. Silva, S.; Almeida, A.J.; Vale, N. Combination of cell-penetrating peptides with nanoparticles for therapeutic application: A review. *Biomolecules* **2019**, *9*, 22. [CrossRef] [PubMed]
42. Herce, H.D.; Schumacher, D.; Schneider, A.F.L.; Ludwig, A.K.; Mann, F.A.; Fillies, M.; Kasper, M.A.; Reinke, S.; Krause, E.; Leonhardt, H.; et al. Cell-permeable nanobodies for targeted immunolabelling and antigen manipulation in living cells. *Nat. Chem.* **2017**, *9*, 762–771. [CrossRef] [PubMed]
43. Taghizadeh, S.M.; Moghimi-Ardakani, A.; Mohamadnia, F. A statistical experimental design approach to evaluate the influence of various penetration enhancers on transdermal drug delivery of buprenorphine. *J. Adv. Res.* **2015**, *6*, 155–162. [CrossRef] [PubMed]
44. Alzubaidi, A.F.A.; El-Helw, A.-R.M.; Ahmed, T.A.; Ahmed, O.A.A. The use of experimental design in the optimization of risperidone biodegradable nanoparticles: In vitro and in vivo study. *Artif. Cells Nanomed. Biotechnol.* **2017**, *45*, 313–320. [CrossRef]

45. Zidan, A.S.; Ahmed, O.A.A.; Aljaeid, B.M. Nicotinamide polymeric nanoemulsified systems: A quality-by-design case study for a sustained antimicrobial activity. *Int. J. Nanomed.* **2016**, *11*, 1501–1516. [CrossRef]
46. Bhattacharjee, S. DLS and zeta potential—What they are and what they are not? *J. Control. Release* **2016**, *235*, 337–351. [CrossRef] [PubMed]
47. Castell, J.V.; Jover, R.; Martínez-Jiménez, C.P.; Gómez-Lechón, M.J. Hepatocyte cell lines: Their use, scope and limitations in drug metabolism studies. *Expert Opin. Drug Metab. Toxicol.* **2006**, *2*, 183–212. [CrossRef]
48. Gerets, H.H.J.; Hanon, E.; Cornet, M.; Dhalluin, S.; Depelchin, O.; Canning, M.; Atienzar, F.A. Selection of cytotoxicity markers for the screening of new chemical entities in a pharmaceutical context: A preliminary study using a multiplexing approach. *Toxicol. Vitr.* **2009**, *23*, 319–332. [CrossRef]
49. Elsayed, M.; Kobayashi, D.; Kubota, T.; Matsunaga, N.; Murata, R.; Yoshizawa, Y.; Watanabe, N.; Matsuura, T.; Tsurudome, Y.; Ogino, T.; et al. Synergistic antiproliferative effects of zoledronic acid and fluvastatin on human pancreatic cancer cell lines: An in Vitro study. *Biol. Pharm. Bull.* **2016**, *39*, 1238–1246. [CrossRef] [PubMed]
50. Salis, O.; Bedir, A.; Gulten, S.; Okuyucu, A.; Kulcu, C.; Alacam, H. Cytotoxic effect of fluvastatin on MCF-7 cells possibly through a reduction of the mRNA expression levels of SGK1 and CAV1. *Cancer Biother. Radiopharm.* **2014**, *29*, 368–375. [CrossRef] [PubMed]
51. Sławińska-Brych, A.; Zdzisińska, B.; Kandefer-Szerszeń, M. Fluvastatin inhibits growth and alters the malignant phenotype of the C6 glioma cell line. *Pharmacol. Rep.* **2014**, *66*, 121–129.
52. Ishikawa, S.; Hayashi, H.; Kinoshita, K.; Abe, M.; Kuroki, H.; Tokunaga, R.; Tomiyasu, S.; Tanaka, H.; Sugita, H.; Arita, T.; et al. Statins inhibit tumor progression via an enhancer of zeste homolog 2-mediated epigenetic alteration in colorectal cancer. *Int. J. Cancer* **2014**, *135*, 2528–2536. [CrossRef]
53. Nishiya, M.; Yasuhira, S.; Shibazaki, M.; Oikawa, H.; Masuda, T.; Maesawa, C. Fluvastatin exerts an antitumor effect in vemurafenib-resistant melanoma cells. *Anticancer. Drugs* **2019**, *30*, 451–457. [CrossRef]
54. Oku, Y.; Nishiya, N.; Sugiyama, S.; Sato, H.; Uehara, Y. Sensitisation of cancer cells to MLN8237, an aurora-a inhibitor, by YAP/TAZ inactivation. *Anticancer Res.* **2018**, *38*, 3471–3476. [CrossRef] [PubMed]
55. Cheng, Y.; Luo, R.C.; Zheng, H.; Wang, B.; Liu, Y.H.; Liu, D.L.; Chen, J.Z.; Xu, W.F.; Li, A.M.; Zhu, Y. Synergistic anti-tumor efficacy of sorafenib and fluvastatin in hepatocellular carcinoma. *Oncotarget* **2017**, *8*, 23265–23276. [CrossRef] [PubMed]
56. Hassanabad, A.F. Current perspectives on statins as potential anti-cancer therapeutics: Clinical outcomes and underlying molecular mechanisms. *Transl. Lung Cancer Res.* **2019**, *8*, 692–699. [CrossRef] [PubMed]
57. Bocci, G.; Fioravanti, A.; Orlandi, P.; Bernardini, N.; Collecchi, P.; Del Tacca, M.; Danesi, R. Fluvastatin synergistically enhances the antiproliferative effect of gemcitabine in human pancreatic cancer MIAPaCa-2 cells. *Br. J. Cancer* **2005**, *93*, 319–330. [CrossRef] [PubMed]
58. Carlin, C.M.; Peacock, A.J.; Welsh, D.J. Fluvastatin inhibits hypoxic proliferation and p38 MAPK activity in pulmonary artery fibroblasts. *Am. J. Respir. Cell Mol. Biol.* **2007**, *37*, 447–456. [CrossRef] [PubMed]
59. Yang, J.D.; Nakamura, I.; Roberts, L.R. The tumor microenvironment in hepatocellular carcinoma: Current status and therapeutic targets. *Semin. Cancer Biol.* **2011**, *21*, 35–43. [CrossRef]
60. Ehlers, M.R.; Todd, R.M. Todd Genesis and Maintenance of Attentional Biases: The Role of the Locus Coeruleus-Noradrenaline System. *Neural Plast.* **2017**, *1*, 2–3.
61. Choi, H.W.; Shin, P.G.; Lee, J.H.; Choi, W.S.; Kang, M.J.; Kong, W.S.; Oh, M.J.; Seo, Y.B.; Kim, G. Do Anti-inflammatory effect of lovastatin is mediated via the modulation of NF-κB and inhibition of HDAC1 and the PI3K/Akt/mTOR pathway in RAW264.7 macrophages. *Int. J. Mol. Med.* **2018**, *41*, 1103–1109.
62. Kilk, K.; Mahlapuu, R.; Soomets, U.; Langel, Ü. Analysis of in vitro toxicity of five cell-penetrating peptides by metabolic profiling. *Toxicology* **2009**, *265*, 87–95. [CrossRef]

63. Dabrowska, A.; Kim, N.; Aldovini, A. Tat-Induced FOXO3a Is a Key Mediator of Apoptosis in HIV-1-Infected Human CD4 + T Lymphocytes. *J. Immunol.* **2008**, *181*, 8460–8477. [CrossRef]
64. Romani, B.; Engelbrecht, S.; Glashoff, R.H. Functions of Tat: The versatile protein of human immunodeficiency virus type 1. *J. Gen. Virol.* **2010**, *91*, 1–12. [CrossRef]
65. Zheng, L.; Da Yang, Y.; Lu, G.C.; Salvato, M.S. Extracellular HIV Tat and Tat cysteine rich peptide increase CCR5 expression in monocytes. *J. Zhejiang Univ. Sci.* **2005**, *6*, 668–672. [CrossRef] [PubMed]
66. Chauhan, A.; Turchan, J.; Pocernich, C.; Bruce-Keller, A.; Roth, S.; Butterfield, D.A.; Major, E.O.; Nath, A. Intracellular human immunodeficiency virus Tat expression in astrocytes promotes astrocyte survival but induces potent neurotoxicity at distant sites via axonal transport. *J. Biol. Chem.* **2003**, *278*, 13512–13519. [CrossRef] [PubMed]
67. Nakajima, H.; Mizuta, N.; Fujiwara, I.; Sakaguchi, K.; Ogata, H.; Magae, J.; Yagita, H.; Koji, T. Blockade of the Fas/Fas ligand interaction suppresses hepatocyte apoptosis in ischemia-reperfusion rat liver. *Apoptosis* **2008**, *13*, 1013–1021. [CrossRef]
68. Evans, G.S. Copper toxicity affects proliferation and viability of human hepatoma cells (HepG2 line). *Hum. Exp. Toxicol.* **2000**, *19*, 367–376.
69. Mazel, M.; Clair, P.; Rousselle, C.; Vidal, P.; Scherrmann, J.M.; Mathieu, D.; Temsamani, J. Doxorubicin-peptide conjugates overcome multidrug resistance. *Anticancer. Drugs* **2001**, *12*, 107–116. [CrossRef]
70. Rousselle, C.; Smirnova, M.; Clair, P.; Lefauconnier, J.M.; Chavanieu, A.; Calas, B.; Scherrmann, J.M.; Temsamani, J. Enhanced delivery of doxorubicin into the brain via a peptide-vector-mediated strategy: Saturation kinetics and specificity. *J. Pharmacol. Exp. Ther.* **2001**, *296*, 124–131.
71. Lindgren, M.; Rosenthal-Aizman, K.; Saar, K.; Eiríksdóttir, E.; Jiang, Y.; Sassian, M.; Östlund, P.; Hällbrink, M.; Langel, Ü. Overcoming methotrexate resistance in breast cancer tumour cells by the use of a new cell-penetrating peptide. *Biochem. Pharmacol.* **2006**, *71*, 416–425. [CrossRef] [PubMed]
72. Foged, C.; Nielsen, H.M. Cell-penetrating peptides for drug delivery across membrane barriers. *Expert Opin. Drug Deliv.* **2008**, *5*, 105–117. [CrossRef]
73. Higashi, T.; Hayashi, H.; Kitano, Y.; Yamamura, K.; Kaida, T.; Arima, K.; Taki, K.; Nakagawa, S.; Okabe, H.; Nitta, H.; et al. Statin attenuates cell proliferative ability via TAZ (WWTR1) in hepatocellular carcinoma. *Med. Oncol.* **2016**, *33*, 123. [CrossRef]
74. Chang, Y.L.; Huang, L.C.; Chen, Y.C.; Wang, Y.W.; Hueng, D.Y.; Huang, S.M. The synergistic effects of valproic acid and fluvastatin on apoptosis induction in glioblastoma multiforme cell lines. *Int. J. Biochem. Cell Biol.* **2017**, *92*, 155–163. [CrossRef]
75. Qi, X.F.; Zheng, L.; Lee, K.J.; Kim, D.H.; Kim, C.S.; Cai, D.Q.; Wu, Z.; Qin, J.W.; Yu, Y.H.; Kim, S.K. HMG-CoA reductase inhibitors induce apoptosis of lymphoma cells by promoting ROS generation and regulating Akt, Erk and p38 signals via suppression of mevalonate pathway. *Cell Death Dis.* **2013**, *4*, e518. [CrossRef]
76. Lin, C.K.; Liu, S.T.; Chang, C.C.; Huang, S.M. Regulatory mechanisms of fluvastatin and lovastatin for the p21 induction in human cervical cancer HeLa cells. *PLoS ONE* **2019**, *14*, e0214408. [CrossRef]
77. Kruman, I.I.; Nath, A.; Mattson, M.P. HIV-1 protein tat induces apoptosis of hippocampal neurons by a mechanism involving caspase activation, calcium overload, and oxidative stress. *Exp. Neurol.* **1998**, *154*, 276–288. [CrossRef]
78. Taylor-Harding, B.; Orsulic, S.; Karlan, B.Y.; Li, A.J. Fluvastatin and cisplatin demonstrate synergistic cytotoxicity in epithelial ovarian cancer cells. *Gynecol. Oncol.* **2010**, *119*, 549–556. [CrossRef]
79. Porter, A.G.; Jänicke, R.U. Emerging roles of caspase-3 in apoptosis. *Cell Death Differ.* **1999**, *6*, 99–104. [CrossRef]
80. Sgonc, R.; Gruber, J. Apoptosis detection: An overview. *Exp. Gerontol.* **1998**, *33*, 525–533. [CrossRef]
81. Kiechle, F.L.; Zhang, X. Apoptosis: Biochemical aspects and clinical implications. *Clin. Chim. Acta* **2002**, *326*, 27–45. [CrossRef]
82. Stepanenko, A.A.; Dmitrenko, V. V Pitfalls of the MTT assay: Direct and off-target effects of inhibitors can result in over/underestimation of cell viability. *Gene* **2015**, *574*, 193–203. [CrossRef]

83. Gonzalez, O.; Iriarte, G.; Rico, E.; Ferreirós, N.; Maguregui, M.I.; Alonso, R.M.; Jiménez, R.M. LC-MS/MS method for the determination of several drugs used in combined cardiovascular therapy in human plasma. *J. Chromatogr. B Anal. Technol. Biomed. Life Sci.* **2010**, *878*, 2685–2692. [CrossRef]
84. Van Engeland, M.; Nieland, L.J.W.; Ramaekers, F.C.S.; Schutte, B.; Reutelingsperger, C.P.M. Annexin V-affinity assay: A review on an apoptosis detection system based on phosphatidylserine exposure. *Cytometry* **1998**, *31*, 1–9. [CrossRef]